H.H. Grotheer, K. Hoffmann, K. Wolf, S. Kanjarkar, C. Wahl, M. Aigner, Study of carbonaceous nanoparticles in premixed C_2H_4-air flames and behind a spark ignition engine, Combust. Flame 156 (2009) 791-800.

The original publication is available at www.elsevier.com

http://dx.doi.org/10.1016/j.combustflame.2009.01.022

Study of carbonaceous nanoparticles in premixed C_2H_4-air flames and behind a spark ignition engine

Horst-Henning Grotheer[1], Kai Hoffmann, Katrin Wolf, Santosh Kanjarkar, Claus Wahl and Manfred Aigner

Institute of Combustion Technology, DLR, Pfaffenwaldring 38, 70569 Stuttgart

Shortened title: Nanoparticles in flames and behind an SI engine

Full-length paper

[1] Corresponding author. Fax +49 711 6862 578. phone +49 711 6862 378, E-mail address: hh.grotheer@dlr.de

Abstract

Nanoparticle size distributions and their concentrations were studied in atmospheric premixed ethylene/air flames using photo ionization mass spectrometry (PIMS) and total organic carbon (TOC) calibration supplemented by differential mobility analysis (DMA). Focus of this study is the evolution of nanoparticles as a function of height above burner (HAB) and of the C/O ratio of the unburned gases. It was found that especially particles of the cluster type exhibit a sharp concentration drop by more than two orders of magnitude within a narrow C/O window which is close to the sooting threshold. Using DMA a decline by two orders of magnitude was found. These results suggest that at best only small concentrations of nanoparticles should be formed significantly below the sooting threshold. As these conditions prevail in a homogeneously charged IC engine no or only very small nanoparticle emissions are expected in the exhaust gas. This was indeed found for a small Otto engine driving a power generator unit. Using flame nanoparticle profiles as standard, absolute concentrations for their emissions could be deduced. These data were supported by additional DMA measurements. The calibration using TOC did not completely match the one based on the condensation particle counter of the DMA apparatus.

Keywords: Soot precursors, nanoparticles, formation threshold, photoionization mass spectrometry, DMA, SI engines

1. Introduction

The existence of carbonaceous nanoparticles (soot precursors) as a species between polyaromatic hydrocarbons (PAHs) and young soot is now widely accepted and has been

demonstrated by a variety of groups using different experimental methods. A more detailed review was recently given by our group [1] so that only a few examples are highlighted here.

As early as 1973 Wersborg et al. [2] discovered extremely small nanoparticles (diameters down to 1.5 nm) as ions behind low pressure C_2H_2/O_2 flames. Subsequently, for a large variety of flame conditions nanoparticles were found using very diverse measurement methods such as UV extinction and fluorescence (D'Alessio et al. [3, 4]), transmission electron microscopy, TEM (Vander Wal [5], Dobbins [6]) and laser microprobe mass spectrometry, LMMS (Dobbins et al. [7]). Several new methods for nanoparticle measurement have been worked out more recently by researchers from Naples, including atomic force microscopy, AFM (Barone et al. [8]), electrospray differential mobility analysis, EDMA (Sgro et al, [9]), and size exclusion chromatography, SEC (Apicella et al. [10]). Further progress with regard to differential mobility analysis (DMA) has been achieved through improved sampling techniques [11, 12]. This made it possible to reliably measure particle sizes down to 2.4 nm. Using these improved techniques it could be shown behind sooting ethylene flames that under certain conditions particle size distribution functions (PSDF) are bimodal, with the two modes being separated by a "valley" around 6 nm [13]. In this context bimodality means that soot precursor particles are regarded as one mode and soot as the other one. Minutolo et al. [14] have pushed the lower size limit of DMA even to 2 nm. Photo ionization as a method to cover the entire range from molecules to young soot was introduced by our group [15] and it showed the existence of soot precursing nanoparticles as a species between PAHs and soot.

Contrary to this clear evidence of nanoparticles it is much more under debate whether a minimum C/O ratio comparable to the sooting threshold is required for the formation of these particles. In a series of papers by D'Alessio and coworkers [3, 16 - 19] premixed ethylene/air flames (C/O = 0.4 to 0.9) were studied. For these flames the yellowish luminosity occurs for C/O >~ 0.6. By contrast, nanometer-sized particles, called transparent soot, were reported to

appear at the C/O ratio as small as 0.4. Interpretation of the UV absorption and scattering data led to the conclusion that for C/O = 0.5 to 0.7 the particles remain around 2.5 nm in diameter and have a number density of ~10^{13} cm^{-3}. For C/O > 0.7, the mean particle size begins to increase with an increase in the C/O ratio [17]. It was noted that the transparent soot is composed by functionalities of two- and three-ring aromatics.

However, in a joint paper of our group and Wang and coworkers [20] combining mass spectrometry and DMA measurements, a concentration drop of soot precursor particles was found to occur in a C/O window adjacent to the sooting threshold. To reconcile these data with the results of D'Alessio et al. reported above it was later suggested [21, 22] that there might be a coexistence of two types of particles, i.e. (i) a cluster-like species as suggested by Violi et al. [23] with a more molecular character formed well below the sooting threshold and to which single photon mass spectrometry may be blind and (ii) a stack-like species which is predominantly detected by PIMS and which is only generated above the sooting threshold. In other words it was assumed that PIMS might have detected the stacks while missing the clusters. The concept of stacks was supported by three experimental findings [21, 22], (i) H/C analysis revealed that the subunits consist of pericondensed PAHs, (ii) their mass spectra show up as patterns typical of oligomers, (iii) this is accompanied by a shift in ionization energy which can be explained by a layered structure, whereas chain-like structures should leave ionization energies basically unchanged.

In a later study [24] it was indeed found that these two particle modes can coexist and that they can be detected and discerned by PIMS provided that the fluence of the ionizing photons is sufficiently low (see Discussion, 4.3). Based on an analysis of the photoionization order [24] the higher mode was identified as stack mode. The lower mode was assumed to consist of cluster-like species as proposed by Violi [23]. As an extension of our earlier paper [20] the C/O dependence of the formation of both types of particles is studied in the present paper.

Because of their practical importance these experiments are supplemented by additional measurements behind a small Otto engine.

2. Experimental setup and methods

For the measurements samples were taken from either flames or from engine exhaust gas. The apparatus is shown in Fig. 1 and described in some detail in a recent paper [24]. Therefore, only a brief description is given here.

2.1 Burner

A so-called McKenna burner was used at atmospheric pressure. It could be positioned relative to the probe in lateral and vertical directions by means of screw drives. The combustion gases were allowed to mix within a sufficiently long duct and were driven through a water-cooled porous bronze disc of 6 cm diameter. The upper part of the flame was stabilized by a steel plate, mounted 30 mm above the porous disk, see Fig. 1. The combustion gases were C_2H_4 (grade 3.0) and compressed air cleaned by an oil filter. When adjusting C/O the gas flows were varied in such a way that the total cold gas flow was always 9.92 slm (standard liters per minute) yielding a cold gas flow velocity of 7.5 cm/s. Gas flows were measured using flow controllers (Tylan) calibrated by means of a coriolis flow meter (Danfoss). No outer co-flow was used. The reaction zone of the flames was attached to the burner. For C/O ratios above 0.62 the sooting zone was observed at heights larger than about 7 mm (see also Fig. 1) and this did not change significantly within the C/O range covered in this study. For the measurements of particles as a function of C/O the probe was positioned at HAB = 15 mm and was thus well within the sooting zone

2.2 Sampling device

A fast flow sampling system was used to suppress undesired reactions in the sampling line. Sample gas is sucked through a nozzle (1.0 mm diameter, choked flow) into a quartz or stainless steel tube (5 mm id). The sampling probe was inserted vertically into the flame in order to reduce flame perturbation. In earlier experiments we used also a horizontal arrangement which actually led to a more pronounced visible disturbance. The experimental results, however, were the same for both geometries. The length of the sampling line was kept as short as possible, typically below 50 cm. Pressures in the sampling tube were between 15 and 55 mbar, the higher pressures were used when a more intense molecular beam was needed. Consequently, the concentration reduction of our sample gas was smaller than in earlier studies. The concentration drop together with short residence times (of only several ms) led to a reduced influence of fast subsequent reactions. A disadvantage of this sampling method is that it needs relatively large sample gas flows of up to 2.5 slm. Furthermore, as with any intrusive method, a disturbance through the probe cannot be excluded when measuring small laboratory flames. Clogging of the nozzle by soot was not a problem since we used only moderately rich flames and because of the short measurement times of about 90 s for a single run.

Approximately 10 cm downstream of the sampling nozzle carrier gas He was mixed to the flow as shown in Fig. 1. This greatly improved the molecular beam intensities. In addition, it cooled the hot sample gases and improved the reliable operation of the pulsed inlet valve. Moreover, to avoid heat-up of the MS a sampling protocol was followed using defined cooling intervals between measurements.

For the engine experiments stainless steal nozzles of the same geometry (nozzle diameter 1.0 mm) were used.

The sample gas flow was checked periodically through an extra flow controller connected to the exhaust port of the sampling line pump.

2.3 PIMS

A modified Parker Series 9 pulsed valve (see Fig. 1) discharged small portions of the sample gas into the mass spectrometer, a commercial reflectron time-of-flight MS, supplied by S. Kaesdorf, Munich, Germany. It was equipped with a photoionization source (ArF excimer laser, nominally 1 to 5 mJ per pulse, 10 ns duration). Photoionization took place in a 6 mm wide light sheet which was orthogonal to the MS axis. No lens was used, rather, through a series of neutral density filters the laser beam could be attenuated to yield photon fluences as low as 10 kW/cm². The MS was modified (ion deflection plates and ion post-acceleration to 10 keV) to facilitate the detection of heavier ions. This was successful for ions up to 600.000 u.

The mass scale of our MS is known through frequent calibrations. Mass spectra shown in this paper typically represent ensemble-averages of 10,000 individual laser shots. For particle measurements they were always recorded as envelopes. This is a reasonable approach as under optimized conditions the mass resolution of this particular MS does not exceed $R = M/\Delta M \sim 1500$ so that even for the lighter particles of this study ($m/e \sim 2000$) unity-resolution cannot be achieved. In an attempt to improve sensitivity we therefore deliberately renounced resolution and increased the bin width of the multi-scaler of the detection system to 512 ns. The smallest available binwidth of the scaler is just 1 ns.

2.4 Differential mobility analyser (DMA)

DMA was used as a second and independent method to support the mass spectrometric data. Our DMA consists of a sampling device designed for minimal subsequent reactions and a differential mobility analyzer coupled to a condensation particle counter (CPC). Details concerning apparatus and measurement procedure have been described in a recent paper [26] so that only a brief description needs to be given here. The sample probe is a 6 mm stainless

steel tube with a lateral hole. In the lower C/O range a diameter of 0.4 mm was used and 0.6 mm for C/O > 0.68. The probe was positioned horizontally in the flame such that the hole faces the center of the burner matrix. A high N_2 flow through the probe provided immediate dilution of the sample. Further downstream more dilution stages are available. Dilution ratios were in the order of 10.000. They were determined from measuring the amount of CO_2 from a stoichiometric flame using FTIR. The sampling system was connected to the DMA apparatus using silicone conductive tubing (5.1 mm id, 600 mm length). Differential mobility analysis was performed using a TSI SMPS model 3080 consisting of a Kr-85 bipolar charger, a nano DMA model 3085 and an ultrafine condensation particle counter (CPC). DMA measurements were carried out under high flow conditions (1.5 l/min).

2.5 Concentration calibration

A drawback of mass spectrometry is that with regard to concentrations only relative results are obtained since in general the relationship between ion count and mass concentration of the sample is not known. To overcome this difficulty a calibration method for C numbers was adopted from Sgro et al. [9]. Here it was used for the determination of particle concentrations. To this end three traps (commercial impingers, cooled by liquid nitrogen) were mounted in series to avoid breakthrough. For the sampling the same nozzle and the same geometry were used as for the MS measurements, i.e. the flame conditions did not change. A total flow of typically 10 Nl sample gas was drawn and this required about 10 minutes. After dewing of the condensate each trap was rinsed with distilled water to obtain a solution/emulsion of 5 ml volume in total. Soot was removed by filtering with a filter (Macherey-Nagel MN85/70). The remaining clear solution was analyzed for carbon. It should contain only small amounts of PAHs for reasons of solubility and only clusters (see later) since stacks are reported to be insoluble in water [25].

Consequently, the amount of measured TOC was attributed to clusters. Using

$$TOC \sim M_{Cluster},$$

i.e. neglecting the mass contribution of H atoms one obtains

$$N_{Cluster} = TOC_{sample} \cdot \frac{\sum_i j^+_{m_i}}{\sum_i j^+_{m_i} \cdot m_i} \qquad \text{Eq. (1)}$$

$N_{Cluster}$ is the number of clusters at the position of sampling, j_{mi}^+ is the number of ion counts in a mass bin (see below). The sums extend over the given mode, m, and are directly taken from the experimental data. TOC_{sample} is the carbon concentration at the sampling point expressed in atomic mass units per cm^3. It is derived from the TOC measured under standard conditions by making use of the sample gas flow measured directly through a flow meter at the exhaust of the sampling point and assuming a temperature of 1500 K at the entrance of the choked sampling nozzle.

Flame profiles so calibrated were also used to calibrate engine emission profiles (see Results, 3.4). In this case measurements have to be compared that refer to different temperatures at the location of sampling. To account for this the following approach was used. For the flame gas (state 1) the equation holds

$$\sum_1 j_i^+ m_i = S_1 \cdot TOC \quad .$$

S is the temperature dependent sensitivity of the measurement device. Similarly one can write for the exhaust gas (state 2)

$$\sum_2 j_i^+ m_i = S_2 \cdot Em \quad ,$$

Em being the emission number density.

In both cases sample inlet nozzles of the same diameter are used, operating at the same pressure and under choked conditions. Then the mass flow rates through the nozzle vary as $(T)^{-0.5}$ and one obtains

$$Em = TOC \cdot \frac{\sum_{2} j_i^{+} m_i}{\sum_{1} j_i^{+} m_i} \cdot \frac{S_1}{S_2} = TOC \cdot \frac{\sum_{2} j_i^{+} m_i}{\sum_{1} j_i^{+} m_i} \cdot \left(\frac{T_2}{T_1} \right)^{1/2} \quad \text{Eq. (2).}$$

The uncertainty of TOC determinations is fairly large and is estimated to amount a factor of 3 in either direction. A further uncertainty lies in the assumptions concerning solubility. Cluster-type particles are assumed to be completely soluble in water whereas stack-like particles as well as PAHs are assumed to be completely insoluble. Therefore the DMA was particularly useful as an independent method for calibration.

2.6 Otto engine

For the investigation of Otto engine exhaust gases a small single-cylinder, 4-stroke engine was used with a displacement of 80.7 ml, bore * stroke being 52 * 38 mm. It is equipped with a carburettor to furnish a gasoline air mixture which is supposed to be homogeneous. No EGR is used. This engine is connected to an electric power generator with a rated power of 2.4 kW at 4000 rpm. Normally our experiments were run under idle and full load conditions by varying the electric load. As fuel we used a reference fuel, CEC Legislative Fuel RF-02-03 with an oxygen content < 0.1%, mass basis, supplied by Haltermann Products, Hamburg, Germany.

2.7 Transformation of a time-of-flight spectrum to a particle mass distribution function (PMDF) or a size distribution function (PSDF)

The subsequent considerations are normally ignored in the literature on mass spectrometry and this is possible since quite often only narrow mass ranges are involved. In our case of

masses ranging into the 100.000 u region, however, more accurate relationships are required to transform the measured time of flight spectra into mass or size distributions. Using a TOF MS with a multi-scaler, spectra are obtained as ion counts per bin. A bin corresponds to a constant time interval during which ions are counted and which can be selected between 1 ns and several µs. Normally, time-of-flight spectra are converted to mass spectra by making use of the relationship

$$Ee = \tfrac{1}{2} \cdot m \cdot v^2 \text{, hence}$$

$$m = 2 \cdot eE \cdot \frac{t^2}{s^2} \qquad \text{Eq.(3),}$$

m is the ion mass, E the electric field which accelerates the ions into the analyzer of length s, t is the time-of-flight. Ions are assumed to bear just one elementary charge, e.

A program for this simple transformation is furnished by the MS supplier and it is appropriate if the measured ion counts refer to discrete mass peaks. It is not correct, however, if one deals with a continuous mass distribution function since this refers to mass bins of constant size. By contrast, the transformation given above leads to bins of increasing size, i.e.

$$\partial m = 4 \cdot eE \cdot \left(\frac{t}{s^2} \right) \partial t \ ,$$

to which the counted ion numbers refer. This means that for higher masses the counter becomes more sensitive because of the increasing bin width. Therefore, to obtain the ion count function in mass display, j_m^+, the ion counts in time-of-flight display, j_t^+, have to be corrected for this effect, i.e.

$$j_m^+ = j_t^+ \cdot \frac{s^2}{4 \cdot t \cdot eE} \qquad \text{Eq.(4).}$$

Consequently, transformation of a time-of-flight spectrum to a particle mass distribution function (PMDF) consists of applying Eq. (3) to the t-axis and Eq. (4) to the ion count axis.

A particle size distribution function (PSDF), j_D^+, can be calculated from j_m^+ or from j_t^+. Particles are assumed as spheres with diameters D and a homogeneous density ρ. Then

$D = m^{1/3} \cdot \left(\frac{6}{\pi \cdot \rho} \right)^{1/3}$. It follows

$\partial D = \left(\frac{2}{9 \cdot \pi \cdot \rho} \right)^{1/3} \cdot m^{-2/3} \partial m$ Consequently

$j_D^+ = j_m^+ \cdot \left(\frac{9 \cdot \pi \cdot \rho}{2} \right)^{1/3} \cdot m^{2/3}$.

Alternatively, j_D^+ can be derived from j_t^+ in a similar way.

3. Results

3.1 Flames. Nanoparticle profiles as a function of HAB (height above burner)

For these measurements fluences around 100 kW/cm² were generally used in order to avoid fragmentation [24]. In addition, the binwidth was set to 512 ns to accumulate more counts in a single bin. This was obviously at the expense of resolution (see above). Bimodality of carbonaceous nanoparticles can best be seen when the influence of subsequent reactions in the

sampling probe is reduced. This is possible under conditions of only small particle concentrations, i.e. in the immediate vicinity of the sooting threshold of the used C_2H_4/air flame. Samples were drawn from the flame centerline for several heights above the burner (see Fig. 1). Time-of-flight spectra are shown in Fig. 2 as a function of HAB (note: log display of the ion signal). Peaks below 39 µs belong to poorly resolved PAHs, in particular pyrene and coronene. The particle modes are separated through a clear valley around 39-45µs from the gas phase. Based on photo ionization studies [24] the lower mode was identified as cluster ions and the higher mode as stacks. The maxima of stack like particles seem to appear at nearly the same time-of-flight. The cluster maxima, by contrast, show a continuous growth. This is observable through the broadening of the distribution curves towards higher flight times. For the low HAB number (5 mm) a clear separation between both particle modes is observable. It becomes somewhat blurred at increased HAB, when both types of particles show a pronounced intensity enhancement.

Through transformation as described in the previous section PMDF curves are derived as shown in Fig. 3. In comparison to Fig. 2 the intensities of the high mode are now much smaller relative to the low mode. This is a result of the transformation outlined in the previous section, especially Eq.(4).

For the estimation of particles sizes the transformation was used as outlined above. The underlying model assumes that the measured particle masses are homogeneously distributed within spheres. For the relatively low masses of the present study this model is obviously debatable as it ignores any structural influence. For the density a value of 1.0 g/cm³ was used for both types of particles. This value is somewhat lower than the one of 1.2 g/cm³ recommended in the literature [7]. The density used in this study was determined by deducing the volume of young soot from an absolute PSDF (particle size distribution function) measurement of a flame sample using DMA. Subsequently for a second sample obtained under the same conditions the weight was measured gravimetrically. Using this density,

PSDFs were calculated from the mass spectra as shown in Fig. 4. Here the PSDFs of the two types of particles show more comparable widths, similar to those of the time-of-flight spectra in Fig. 2. The reason is that the relationship between time bins and size bins is much closer to linearity than between time bins and mass bins. One notes again that relative to the stacks, the cluster peaks show a more pronounced growth (i.e. shift towards larger sizes) as a function HAB. It is obvious, that the second mode (stack mode) stays more or less at the same mean size of about 3.6 nm. For the cluster mode, however, a continuous growth of the diameters at the peak maxima ranging from 1.62 to 2.15 nm can be extracted from Fig. 4. These are plotted as a function of HAB in Fig. 5

3.2 Flames. Nanoparticle profiles as a function of C/O. PIMS measurements.

With regard to sampling probe, fluence and binwidth these measurements were carried out under the same conditions as the ones described above. For the height above burner a constant value of 15 mm was used and this insured that the sampling probe was always in the region of soot formation (yellow luminescence). The ratio of the unburned gases was varied in such a way that the total gas flow and hence cold gas flow velocity were the same for all experiments. Time-of-flight spectra so obtained are shown in Fig. 6. For C/O = 0.541 and 0.571 we get two coincident profiles. Above 39 μs which was defined above as the time of flight of very light particles, these profiles show continuously declining mass signals. They are interpreted as heavy PAHs. For C/O = 0.602 a convex bump is observed in the region between 39 and 80 μs and is interpreted as particle signal (cluster mode). It becomes more pronounced (note: log scale) for richer mixtures (0.626). Here also week stack signals appear, hardly discernible from noise. At our next C/O value (0.641) a clear bimodal distribution function is observed. The valley between these modes becomes blurred for C/O = 0.657. For even richer mixtures the flanks of the cluster mode shift to higher and higher masses so that a distinction of clusters and stack-like particles becomes difficult. The C/O ratio of 0.602 when

the first clusters show up, agrees well with the sooting threshold of 0.60 as reported in the literature for atmospheric ethylene-air flames [27, 28]. It is this C/O ratio when a faint yellowish luminosity became visible under observation against a black cardboard.

For the sake of brevity mass distribution functions (PMDFs) are not shown and Fig. 7 gives particle size distribution functions (PSDFs) obtained from Fig. 6 as described above.

Finally, the relative numbers of particle ions were evaluated as a function of the C/O ratio. To this end distribution curves (time-of-flight spectra) are integrated with 39 μs being taken uniformly as lower integration limit. The upper limit of the cluster mode and both limits of the stack mode were determined graphically. For higher C/O ratios this led to fairly high uncertainties in particular with regard to the numbers of stack-like particles. The corresponding data are shown in Fig. 8 along with the large uncertainty bars referring to stacks.

For the conversion of the data presented especially in Fig. 8 into number concentrations, a calibration is needed. According to the procedure outlined in section 2.5 it was obtained by measuring the total organic carbon content (TOC) under not too heavily sooting conditions, i.e. C/O = 0.673. Closer to the sooting limit concentrations become very small and can not be determined accurately. A typical result that we obtained for C/O = 0.673 and after sampling of 10 Nl flame gas are carbon concentrations around 82 ppm (relative to water) in the three impingers each of them containing 5ml aequous solution. Assuming a flame temperature of 1500 K in the vicinity of the sampling nozzle, this leads to a TOC value of $4.5*10^{15}$ u/cm³ and by using Eq. (1) to a cluster number density of $9*10^{11}$ cm^{-3}, marked by an arrow in Fig. 8. This calibration can be used for all other conditions as well through the relationship

$$N_y \sim \sum_{mode} j^+_{my} .$$

Since these concentration determinations are not very accurate (see Discussion, 4.9) additional measurements using DMA were carried out.

3.3 Flames. Nanoparticle profiles as a function of C/O. DMA measurements.

For the DMA measurements the same burner and gas supply was used as for the PIMS experiments. In order to cope with the expected broad range of particle number concentrations the degree of N_2 dilution was varied between 1:5,000 and 1:20,000. It was determined through CO_2 measurement using FTIR. Unfortunately, our DMA did not resolve the bimodal nanoparticle distribution found in the C/O window between 0.63 and 0.67. The results for the mean particle diameters and the respective number concentrations are given in Table 1. In Fig. 9 mean diameters obtained with DMA are compared to those deduced from PIMS measurements. Obviously, the DMA diamters are systematically larger. This is interpreted as an indication of coagulation despite of the used high dilution ratios.

For a comparison to the MS data the number concentrations were corrected by applying an equation for mass conservation, i.e.

$$N_{DMA} \cdot d_{DMA}^3 = N_{corr} \cdot d_{MS}^3 ,$$

see fourth column in Table 1. These data are plotted in Fig. 10, upright triangles. Towards the sooting limit a concentration drop is found although somewhat less pronounced in comparison to the MS results. The latter data are also shown in Fig. 10, yet normalized in such a way that an optimum match to the DMA curve is achieved. By so doing the PIMS calibration point ($9*10^{11}$ particles/cm³) shows a value of $3*10^{11}$ on the concentration axis referring to the DMA data. This means that the TOC calibration and the one given by the condensation particle counter differ by a factor of 3, TOC calibration yielding the higher values.

In summary PIMS and DMA measurements show that nanoparticle concentrations (stacks and clusters) exhibit a change by 2 orders of magnitude within a C/O window as narrow as 0.1. This window is adjacent to the sooting limit which therefore appears to be a limit for nanoparticle formation as well. Under the assumption that this feature can be extrapolated

also to other flames, it should be meaningful for other combustors using homogeneous mixtures below the sooting limit as, for example, an Otto engine.

3.4 Otto engine. PIMS measurements.

Since, on an overall basis, SI engines are operated under stoichiometries far below the sooting threshold no or only small nanoparticle concentrations are expected in the exhaust gas. To check for this, conditions were looked for leading to maximum emissions. A series of runs was performed using the engine described in Section 2.6 and fuelled with reference gasoline. Measurements were carried out only after sufficient warm-up of several minutes. In a series of measurement sets it was found that under high load conditions emissions were smaller. Consequently, only results referring to idle conditions are reported here. Also when sampling at the center of the muffler signals were slightly higher than those referring to the tail-end of the exhaust train. Therefore, most of the measurements were carried out at the former position. Results of an exemplary measurement set are shown in Fig. 11 in time-of-flight display (i.e. as measured) and in Fig. 12 in diameter display. Curve I is an average of three profiles measured at the center of the muffler and with the engine running smoothly. At 1.1 nm, there is a small peak possibly indicating the release of very small particles. Otherwise a broad distribution is found exhibiting small signals over a mass range up to several 100.000 u. Under the same conditions, yet measured directly at the cylinder-head, i.e. with the exhaust train being removed, profile II was found showing exactly the same distribution and the signals by about a factor of 2 higher.

In another series of runs the choke was pulled (i.e. richer mixture) to an extent that the engine still operated smoothly. The result, again measured in the center of the muffler, is curve III showing significantly higher signals at smaller masses, yet with a more pronounced decline for higher masses. Also a hump is found at 60μs corresponding to particles of about 1.4 nm.

Curve IV is an average of 5 flame profiles measured for calibration purposes (Hab = 15 mm, C/O = 0.673). To apply Eq. (2) the temperature at the measurement position in the muffler was determined to be T_2 = 533 K and the flame temperature was estimated as T_1 = 1500 K. TOC was 7.5*10^{-9} g/cm³ (extrapolated to flame temperature). The evaluation of $\sum_1 j_i^+ m_i$ from the flame profile data does not present a problem and leads to 1.02*10^{10} u. The value of $\sum_2 j_i^+ m_i$, however, is less clearly defined as it diverges at high mass numbers because of the factors m_i and hence becomes dependent on the choice of the upper summation limit. For an upper limit in terms of time-of-flight of 200 µs (corresponding to about 12.5 ku or a diameter of 3.4 nm) we find for the mass-weighted sum a value of 3.4*10^7 u. Conversely, for a (less realistic) higher time-of-flight of 400 µsec (52 ku, 5.5 nm) this number increases to 9.8*10^7 u, again referring to profile I. Consequently, for the emission any value is possible between

$$Em = 15\,\mu g/m^3 \quad \text{to} \quad 43\,\mu g/m^3 .$$

Under choked conditions the emissions are higher, particularly so for lower masses. The divergence of the mass-weighted sum, however, is less pronounced. For the summation limits quoted above we find

$\sum_2 j_i^+ m_i = 5.4 \cdot 10^8$ u (200 µs limit) and

$\sum_2 j_i^+ m_i = 1.13 \cdot 10^9$ u (400 µs limit) leading to emission values in the order of

$Em = 300\,\mu g/m^3$ in the choked case.

Obviously it is not satisfying that only a range of numbers can be given. In addition, to obtain these data calibration with a flame combined with TOC measurement has been used which may yield too high number densities (see above, Section 3.3) Therefore, additional measurements were carried out using DMA.

3.5 Otto engine. DMA measurements.

Exhaust gas samples were drawn via a 1.5 m heated hose (6 mm i.d.) to a dilution stage and diluted with N_2 (100:1). The connection to the DMA described in Section 2.4 was through a further hose of 2 m length. After a warm-up period of the engine a series of DMA runs was conducted under normal engine conditions (no choke, no load). For comparison also the PSDFs prevailing in ambient air were measured and turned out to be not very different from those of the engine exhaust. For the latter a typical result is shown in Fig. 13 along with data furnished by the statistical DMA program. Although the PSDF of Fig. 13 is broad with no clearly pronounced maximum the statistical data provide a mean size of 16.3 nm and an associated number density of $2.4*10^4$. The total emission is given as 6.2 µg/m³ for the undiluted case. From other measurements we obtained 14.3, 9.9 and 28.0 µg/m³. This leads to

$$Em = 15 + -10 \, \mu g / m^3 .$$

This number is in the same order as those obtained by PIMS. That it is somewhat lower may be caused by the discrepancy between TOC calibration and CPC calibration. In any case this number indicates fairly low emissions.

4. Discussion

4.1 Calibration

As mentioned above in Section 2.5 nanoparticle calibration from TOC determination in an aequous solution rests on the assumptions that nanoparticles (at least those of the cluster type) are completely soluble in water, that this solution does not contain soluble hydrocarbons which would contribute to TOC and that soot can be completely removed by filtering. None of these assumptions has been really proven. Moreover it cannot be excluded that nanoparticles are partly lost by adhesion to soot on the filter. In addition there are losses of

solution in the filter and the filter itself can contribute to TOC. We tried to account for the latter effect through blanc runs. By so doing it is assumed that each filter contributes about the same amount to TOC. In view of all these uncertainties our nanoparticle calibration is at best reliable to a factor of 5.

The uncertainty in the calibration through the DMA apparatus is much smaller. It is predominantly caused by the determination of dilution factors which we estimate to be good within a factor of 2. Consequently, the agreement of both calibration methods within a factor of 3 is fairly good. That we deduce higher nanoparticle concentrations from the TOC method can mean that the used aequous solution contains also carbonaceous gas phase compounds. This issue is under investigation.

4.2 Mass spectrometric sensitivity for nanoparticles

The sensitivity of photoionization mass spectrometers for particle detection is much lower in comparison to mobility analyzers (DMA).An obvious reason is that only a tiny fraction of the sample at atmospheric pressure eventually enters the ion source. Also in comparison to gas phase measurements, PIMS sensitivities are significantly lower for particles. One reason is that for gas phase measurements generally much higher fluences are used for photo ionization, i.e. some MW/cm². Contrary to this, in order to avoid cluster fragmentation we were forced to use fluences around or below 100 kW/cm². This is obviously at the expense of sensitivity. When considering that one measurement typically requires 90 s, it becomes clear that our PIMS method in its present form is not suitable for the monitoring of nanoparticles under transient conditions.

4.3 Comparison to own studies

So far we have studied particles from either low pressure (120 – 180 mbar) flames [1, 15, 20, 21, 22, 29] or atmospheric flames [20, 24, this study]. In particular with regard to the

separation of particle spectra from gas phase spectra there is a difference as for low pressure flames an overlap between these two spectral portions is found [22] whereas for normal pressure flames a clear "valley" shows up between molecular signals and those of particles. The underlying reason is not yet understood and is currently being under investigation.

In comparison to our earlier study dealing with a C/O threshold for nanoparticle formation [20] two major improvements have been achieved:

(i) In the earlier study [20] a cross-beam ion source was used as described by Gonzalez Baquet et al. [30]. This arrangement was often preferred in the earlier MS literature as it reduces contamination of the analyzer and in particular of the detector. The disadvantage is that after ionization the measured species have to be forced to follow the right angle into the analyzer. Obviously, as described in the literature [31] this can lead to losses and especially so at the higher masses. For this reason and since by using a reflectron TOF MS a direct contamination of the multiplier is much less probable, we decided to use an axial source as shown in Fig. 1. This reduces the mass dependence of the sensitivity. As a result the present spectra extend to much higher masses.

(ii) As was found out only recently [24] the fragmentation threshold of cluster-type particles for 193 nm photons is unusually low. For PAHs, laser power densities of 3 MW/cm² can mostly be used without fragmentation [32]. By contrast, cluster-type particles are already destroyed to a significant extent at only 0.2 MW/cm² [24]. The consequence is that in our earlier study [20] by using 0.8 MW/cm² we could only measure stack-type particles, clusters were probably fragmented. This is the reason why in the present paper fluences around or below 0.1 MW/cm² were used. As a consequence this is the first paper to report on MS measurements of the C/O dependence of cluster concentrations.

A further difference to the earlier study [20] is that we now used air as an oxidiser rather than O_2. According to unpublished own work the lower temperatures associated with fuel-air flames favour generation of the cluster mode. For the dependence of stack concentrations on C/O ratios, there is agreement with the earlier paper [20]. The more pronounced dependence of cluster particles is new and is an extension of our earlier work. The conclusion of the earlier paper was that nanoparticle concentrations become vanishingly small when approaching the soot threshold from the rich side. As expected this message was not obscured by the described experimental deficits with regard to stacks. Rather it is augmented through the present study by including clusters as well.

4.4 Size of nanoparticles and especially of stacks

Using mass spectrometers mostly discrete mass peaks are measured and the time-of-flight scale can be easily converted into a mass scale. If, however, time-of-flight distributions are involved the ion count function has to be transformed as well. Normally this is ignored leading to PMDFs that are enhanced at higher masses. In this case the maxima of distribution curves cannot be correctly determined. For PSDFs the error is smaller. For the typical size distributions of this study maxima are shifted by about 10% towards higher values when using the conventional, yet incorrect approach.

An uncertainty in deriving a PSDF from a PMDF arises from the density. For soot precursor particles a density of 1.2 g/cm³ is normally recommended [7] and for soot 1.8 g/cm³. One could also argue that stack like particles with their graphitic structure should have a density close to the one of soot. We have numerically simulated such an effect and the result is that the maxima of the stack mode are shifted by 11 to 12 % to lower diameters. Clusters remain unchanged. In this study a value of 1.0 g/cm³ was used uniformly.

4.5 Comparison to other studies

The information of Figs. 8 and 10 consists of two parts that are related to each other,

(i) a significant change of nanoparticle concentrations within a narrow C/O band close to the sooting threshold,

(ii) below the sooting threshold low concentrations approaching $1*10^9$ particles/cm³ in the case of cluster-type particles for which a calibration could be carried out.

High concentrations in the order of 10^{13} particles/cm³ have been reported in several papers by D'Alessio and coworkes, for instance [4] for a C/O = 0.77 ethylene/air flame and this is well compatible with Figs. 8 and 10. However, in another paper of the same year [17] a nearly constant particle volume fraction of $6*10^{-8}$ is reported for C/O values ranging from 0.48 to 0.72 along with particle mean diameters between 2.2 and 2.6 nm in the same C/O range. For C/O = 0.5 this leads to a number density of $8*10^{12}$cm^{-3}. This high number density below the sooting threshold is not supported by the present results. For C/O = 0.58 and below we find cluster concentrations around $5*10^9$ cm^{-3}, i.e. about 3 orders of magnitude lower.

With regard to the concentration drop the situation is more complex. From DMA data measured as a function of C/O one can infer that indeed a large concentration drop was found by D'Alessio and coworkers [33] in accord with the data presented here. The same applies to a later DMA study from the same laboratory [14] although through the application of several correction factors to the raw data the decline becomes less pronounced. The authors report that their spectroscopic method and DMA yield "a comparable amount of material" for C/O = 0.65. Already for C/O = 0.60, however, the DMA result is two orders of magnitude below the spectroscopic data. Through the agreement of MS data [20] and DMA data [33] this could be interpreted as evidence that the concentrations drop indeed to very small values and that the interpretation of the optical results is incorrect. By contrast, the authors state that their "results remove reasonable doubts on the existence of nanoparticles below soot formation and they strongly reduce the gap between the numbers of nanoparticles estimated by optical methods and by DMA".

With regard to the bimodality of nanoparticles and sizes of the respective modes, there is a good match of our results with data obtained in the laboratory of D'Alessio and coworkers. From Fig. 4 it is evident that we find mean diameters between 1.6 and 2.1 nm for clusters and about 3.6 nm for stacks. This is comparable to "a smallest mode with modal mobility diameter of about 2 nm, a larger and wider mode whose mobility diameter changes from 3 to 4 nm…" as reported by Sgro et al. [25, 34, 35].

With regard to growth dynamics our interpretation is different from the one of D'Alessio and coworkers. In our experiments the high mode shows up at fairly constant sizes whereas the low mode exhibits significant growth as a function of HAB (height above burner) and also when the C/O ratio is raised. This suggests that the low mode represents the growth species eventually leading to soot. In this case of sufficient residence time and sufficiently high C/O the cluster mode obviously becomes the high mass mode

4.6 Meaning for Otto engines

For nanoparticle emissions from practical combustors it is extremely important whether these particles are only formed at C/O ratios above the sooting threshold or already below, eg. at C/O = 0.4. This has been pointed out by D'Alessio and coworkers [4]: "This route of formation of carbonaceous material is relevant to practical nonsooting combustion conditions, like spark-ignited engines or gas turbines, where there is a range of local C/O ratios between the stoichiometric and the soot formation threshold." Indeed, a formation range between slightly rich and the sooting threshold would render these particles inevitable for many kinds of technical combustors.

However, according to the results shown in Figs. 8 and 10 and assuming that they are valid for other flames as well, no pronounced particle emissions are to be expected for an Otto engine using a carburettor nor from any IC engine under conditions of homogeneous charge. Using PIMS we found particle emissions under normal conditions to be in the order of 20

µg/m³. This translates to $6*10^9$ particles/cm³ if tiny monodisperse particles of only 2000 u (corresponding to 1.8 nm) are assumed as a model. This number density is considerably below the value of $1*10^{12}$/cm³ quoted by Sgro et al. [33] for an SI engine and given there "as a proof of concept and not meant to be representative for typical engines".

In a very recent paper Sgro et al. [36] report on measurements behind 2004 model vehicles with CI and SI engines. Several experimental methods were used and absolute nanoparticle concentrations could be derived from extinction measurements. For the two gasoline engines they report 150 µg/m³ and 60 µg/m³, respectively, for the 10:1 diluted exhaust. Using the lower value and assuming 2 nm (i.e. 4000 u) for the particles, a number density of about $1*10^{11}$ cm^{-3} can be derived for the undiluted case. If 3.3 nm particles are assumed the number density drops to about $2*10^{10}$ cm^{-3}. Unfortunately, the discrepancy to the earlier data [33] is not discussed.

Obviously the emission data presented in this study are not only below the early results of Sgro et al. [33] but also below the more recent ones [36]. This is not necessarily a contradiction as it is not known which type of gasoline engine they investigated in their recent paper. For instance, in the case of a directly injected engine and even in a port injection system a slightly less perfect mixture could have resulted leading to local generation of nanoparticles and soot. Nevertheless from the PIMS and DMA data presented in this study, it seems that the jeopardy of nanoparticle emissions is smaller than previously assumed, at least so with regard to homogeneously charged SI engines.

5. Conclusion

Due to the use of very low photoionization fluences both types of nanoparticles could be monitored simultaneously by PIMS. This allowed to measure the concentration dependence of cluster particles on the C/O ratio for the first time. A large concentration drop within a narrow

C/O window close to the sooting threshold was found. Similar data were found using DMA. Extrapolation of this result to other flames leads to the expectation that below the sooting threshold particles should be formed in only very low concentrations and this was verified for a small Otto engine using PIMS supplemented by DMA.

Acknowledgement

We gratefully acknowledge discussions with Dr. K.P. Geigle from our institute.

References

1. H.-H. Grotheer, H. Pokorny, J. Happold, T. Gonzalez Baquet, M. Thierley, M. Aigner, C. Baumstark-Khan, C.E. Hellweg and A. Arenz, Current Nanoscience 3 (2007) 199-206.

2. B.L. Wersborg, J.B. Howard, G.C. Williams, Proc. Combust. Inst. 14 (1973) 929-940.

3. A. D'Alessio, A. D'Anna, A. D'Orsi, P. Minutolo, R. Barbella, A. Ciajolo, Proc. Combust. Inst. 24 (1992) 973-980.

4. P. Minutolo, G. Gambi, A. D'Alessio, A. D'Anna, Combust. Sci. and Tech. 101 (1994) 311-325.

5. R.L. VanderWal, Combust. Flame 112 (1998) 607-616.

6. R.A. Dobbins, in: F.L. Dryer, R.F. Sawyer (Eds.), Physical and Chemical Aspects of Combustion, 1998, pp. 107-133.

7. R.A. Dobbins, R.A. Fletcher, W. Lu, Combust. Flame 100 (1995) 301-309.

8. A.C. Barone, A. D'Alessio, A. D'Anna, Combust. Flame 132 (2003) 181-187.

9. L.A. Sgro, P. Minutolo, G. Basile, A. D'Alessio, Chemosphere 42 (2001) 671-680.

10. B Apicella, A. Ciajolo, I. Suelves, T.J. Morgan, A.A. Herod, R. Kandiyoty, Combust. Sci. and Techn. 174 (2002) 345-359.

11. B. Zhao, Z. Yang, J. Wang, M.V. Johnston, H. Wang, Aerosol Sci. Technol. 37 (2003) 173-188.

12. M.M. Maricq, Combust. Flame 137 (2004) 340-350.

13. B. Zhao, Z. Yang, Z. Li, M.V. Johnston, H. Wang, Proc. Combust. Inst. 30 (2005) 1441-1448.

14. P. Minutolo, A. D'Anna, A. D'Alessio, Combust. Flame 152 (2008) 287-292.

15. H.-H. Grotheer, H. Pokorny, K.L. Barth, M. Aigner, Chemosphere 57 (2004) 1335-1342.

16. A. D'Anna, A. D'Alessio, P. Minatolo, in: H. Bockhorn (Ed.) Soot Formation in

Combustion: Mechanisms and Models of Soot Formation, Springer Series in Chemical Physics 59, Springer-Verlag, Berlin, 1994, pp. 83-103.

17. P. Minutolo, G. Gambi, A. D'Alessio, Proc. Combust. Inst. 27 (1998) 1461-1469.

18. A. D'Alessio, A. D'Anna, G. Gambi, P. Minutolo, J. Aerosol Sci. 29 (1998) 397-409.

19. P. Minutolo, G. Gambi, A. D'Alessio, S. Carlucci, Atmos. Environ. 33 (1999) 2725-2732.

20. M. Thierley, H.-H. Grotheer, M. Aigner, Z. Yang, A. Abid , B. Zhao, H. Wang, Proc. Combust. Inst. 31 (2007) 639-647.

21. J. Happold, H.-H. Grotheer, M. Aigner, *International Workshop on Combustion generated fine Particles 2007,* Anacapri, Italy, May 13-16, to appear as book.

22. J. Happold, H.-H. Grotheer, M. Aigner, Rapid. Commun. Mass Spectrom. 21 (2007) 1247-1254.

23. A. Violi, A.F. Sarofim, T.N. Truong, Combust. Flame 126 (2001) 1506-1515.

24. T. Gonzalez Baquet, H.-H. Grotheer, M. Aigner, Rapid Comm. Mass. Spectrom. 21 (2007) 4060-4064.

25. L.A. Sgro, A. De Filippo, G. Lanzuolo, A. D'Alessio, *International Workshop on Combustion generated fine Particles 2007,* Anacapri, Italy, May 13-16, to appear as book.

26. R. Stirn, T. Gonzalez Baquet, S. Kanjarkar, W. Meier, K.P. Geigle, H.-H. Grotheer, C. Wahl, M. Aigner, Combust. Sci. and Techn. (2008) in press.

27. H. Mätzig, H.Gg. Wagner, Proc. Combust. Inst. 21 (1988) 1047-1055.

28. B.S. Haynes, H.Gg. Wagner, Prog. Energy Combust. Sci. 7 (1981) 229-273.

29. H. Pokorny, M. Thierley, H.-H. Grotheer, M. Aigner, Proc. European Combust. Meeting, 2005, Louvaine, Belgium.

30. T. Gonzalez Baquet, K.-L. Barth, H.-H. Grotheer, M. Aigner, Proc. European Combust. Meeting, 2005, Louvaine, Belgium.

31. U. Zimmermann, U. Näher, S. Frank, T.P. Martin, and N. Malinowsky, in T.P. Martin (Ed.) Large clusters of atoms and molecules, Kluwer Academic Publishers, 1996, pp. 511-530.

32. J. Ahrens, A. Keller, R. Kovacs, and K.H. Homann, Ber. Bunsenges. Phys. Chem. 102 (1998) 1823-1839.

33. L.A. Sgro, G. Basile, A.C. Barone, A. D'Anna, P. Minutolo, A. Borghese, A. D'Alessio, Chemosphere 51 (2003), 1079-1090.

34. L.A. Sgro, A. De Filippo, G. Lanzuolo, A. D'Alessio, Combust. Inst. 31 (2007) 631-638.

35. A. De Filippo, M. Commodo, P. Minutolo, L.A. Sgro, Proc. European Combust. Meeting, (2007) Crete, Greece.

36. L.A. Sgro, A. Borghese, L. Speranza, A.C. Barone, P. Minutolo, A. Bruno, A. D'Anna, and A. D'Alessio, Environ. Sci. Technol. 42 (2008), 859-863.

Figure captions

Fig.1: Sketch of the experimental setup.

Fig. 2: Time-of-flight spectra of nanoparticles as a function of HAB (in mm). Burner/sampling conditions: C/O = 0.64, nozzle 1mm id, quartz tube 4 mm id, flame sample gas 2.4 slm, He 3.3 slm, $p_{\text{pulsed valve}}$ 65 mbar, fluence 90 W/cm².

Fig.3: Data of Fig. 2 transformed to mass display

Fig. 4: PSDFs obtained from Fig. 3 using ρ= 1.0 g/cm³

Fig. 5: Growth of the mean size of the cluster mode (Fig. 4) as a function of HAB

Fig. 6: Time-of-flight spectra of nanoparticles as a function of C/O. HAB = 15 mm. Otherwise burner/sampling conditions as in Fig. 2.

Fig. 7: Particle size distribution functions (PSDF) using the experimental data of Fig. 6.

Fig. 8: Relative particle concentrations as a function of C/O for clusters and stacks. Data from Fig. 6.

Fig. 9 Nanoparticle diameters as function of C/O measured with PIMS and DMA.

Fig. 10 Nanoparticle number density as function of C/O measured with DMA. Also shown is the PIMS curve after normalization.

Fig. 11: Particle time-of-flight spectra behind an Otto engine.

Fig. 12: PSDFs deduced from Fig. 11.

Fig. 13: DMA measurements behind behind an Otto engine.

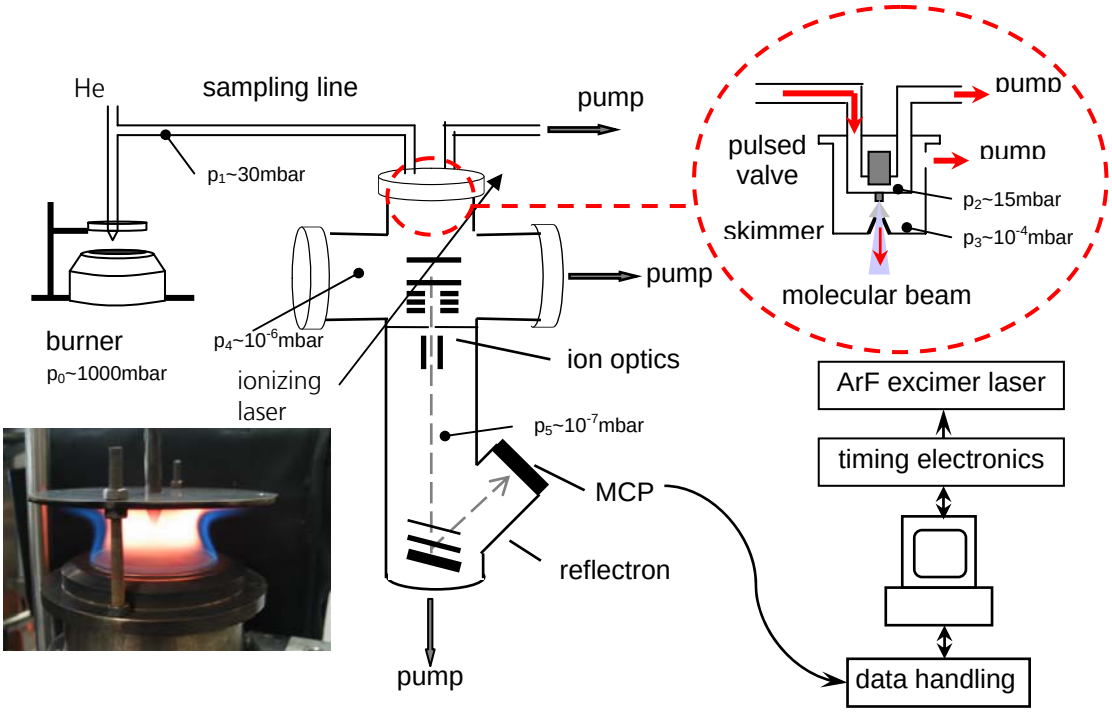
He
sampling line
pump
p1~30mbar
pump
pulsed
valve
pump
skimmer
p2~15mbar
p3~10-4mbar
molecular beam
pump
burner
p0~1000mbar
p4~10-6mbar
ionizing
laser
ion optics
ArF excimer laser
p5~10-7mbar
timing electronics
MCP
reflectron
data handling
pump

Fig. 1

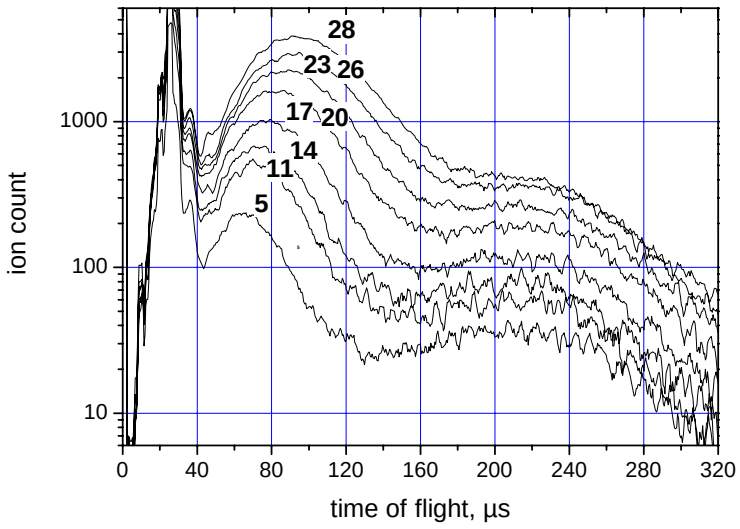
28
23
26
17
20
14
11
5
1000
100
10
ion count
0
40
80
120
160
200
240
280
320
time of flight, µs

Fig. 2

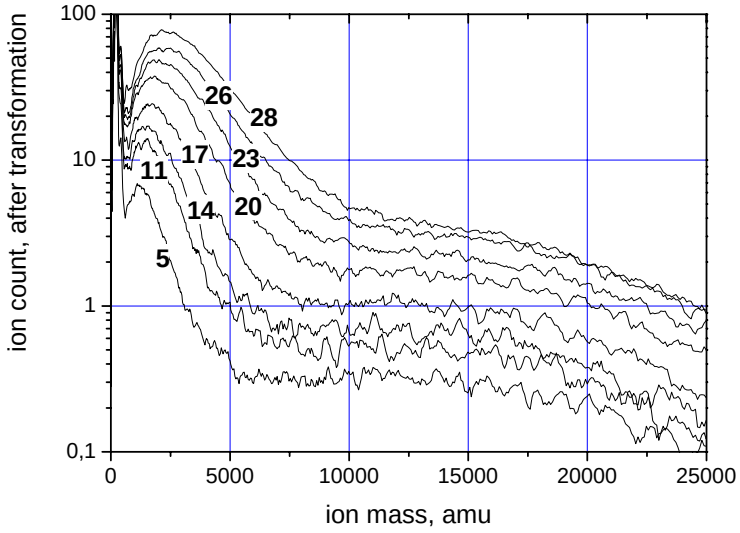
ion count, after transformation
ion mass, amu
100
10
1
0,1
0
5000
10000
15000
20000
25000
26
28
17
23
11
20
14
5

Fig. 3

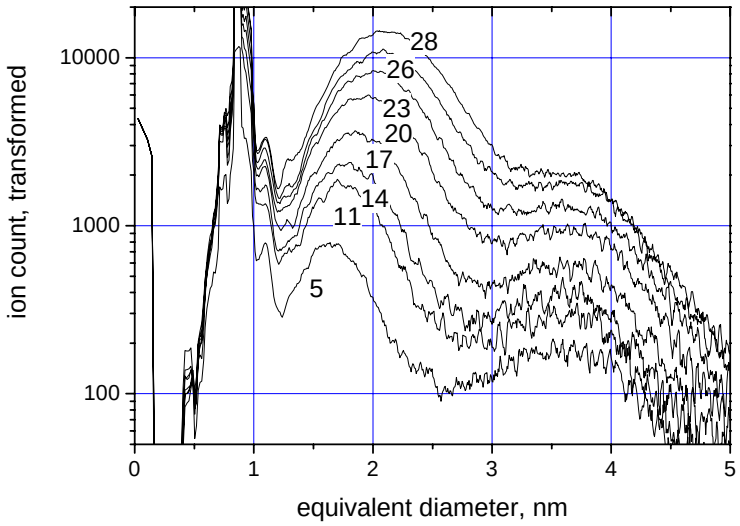
ion count, transformed
equivalent diameter, nm
10000
1000
100
0
1
2
3
4
5
28
26
23
20
17
14
11
5

Fig. 4

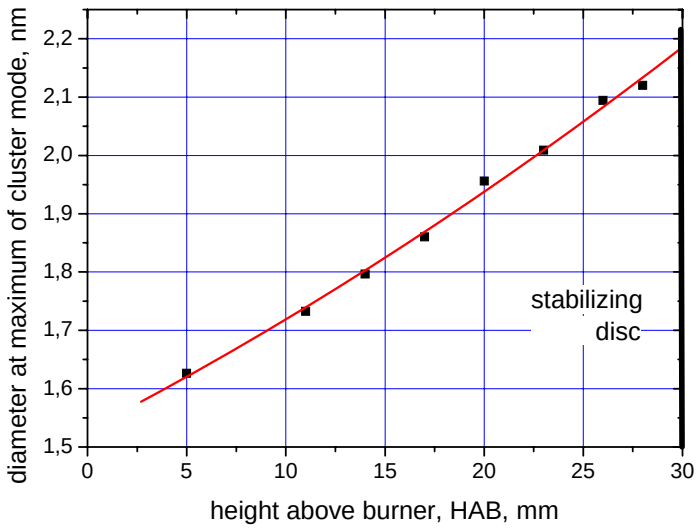
diameter at maximum of cluster mode, nm
2,2
2,1
2,0
1,9
1,8
1,7
1,6
1,5
0
5
10
15
20
25
30
height above burner, HAB, mm
stabilizing
disc

Fig. 5

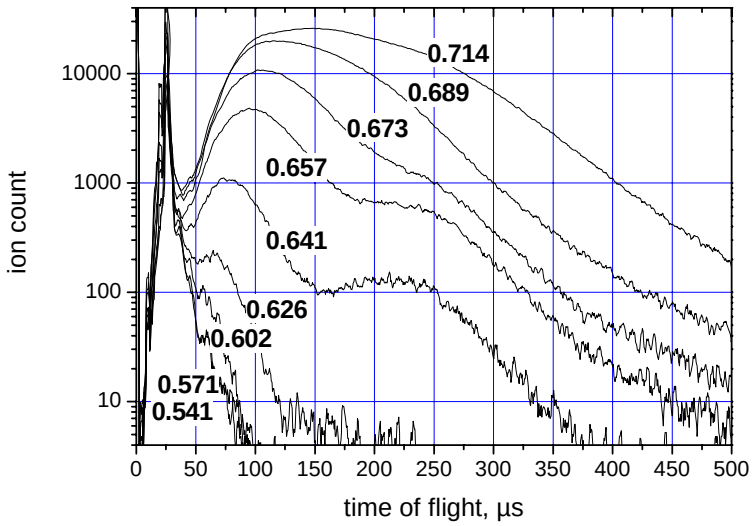
ion count
10000
1000
100
10
0
50
100
150
200
250
300
350
400
450
500
time of flight, µs
0.714
0.689
0.673
0.657
0.641
0.626
0.602
0.571
0.541

Fig. 6

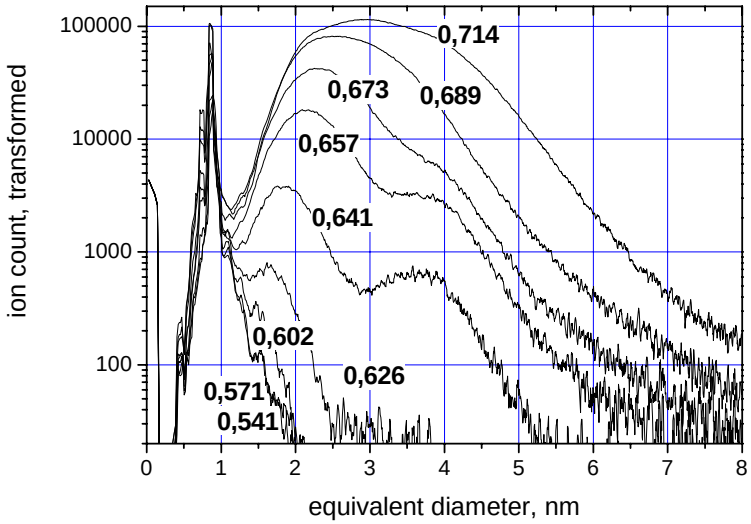
ion count, transformed
100000
10000
1000
100
0,714
0,673
0,689
0,657
0,641
0,602
0,626
0,571
0,541
0
1
2
3
4
5
6
7
8
equivalent diameter, nm

Fig. 7

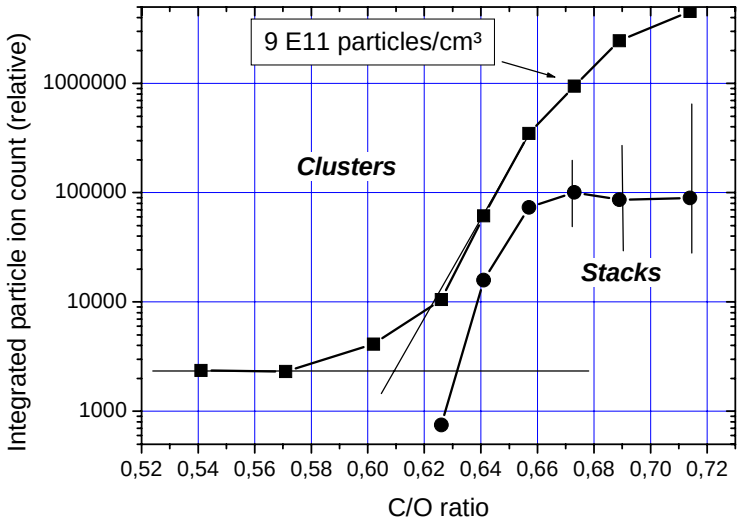
9 E11 particles/cm³
Integrated particle ion count (relative)
1000000
100000
10000
1000
Clusters
Stacks
0,52
0,54
0,56
0,58
0,60
0,62
0,64
0,66
0,68
0,70
0,72
C/O ratio

Fig. 8

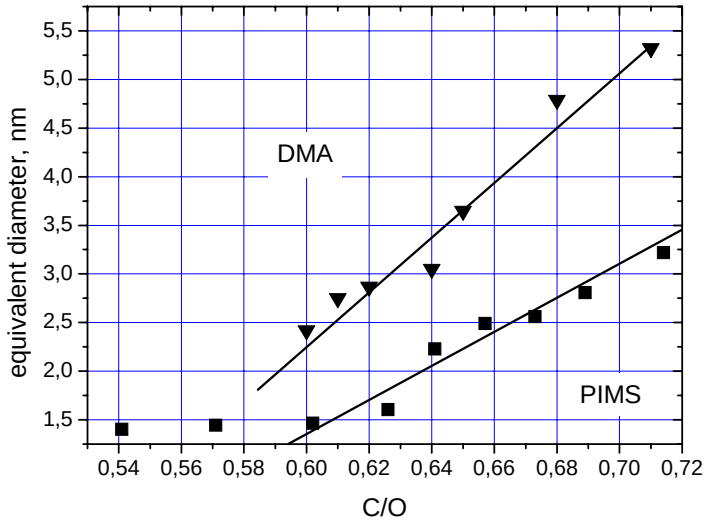
equivalent diameter, nm
5,5
5,0
4,5
4,0
3,5
3,0
2,5
2,0
1,5
DMA
PIMS
0,54 0,56 0,58 0,60 0,62 0,64 0,66 0,68 0,70 0,72
C/O

Fig. 9

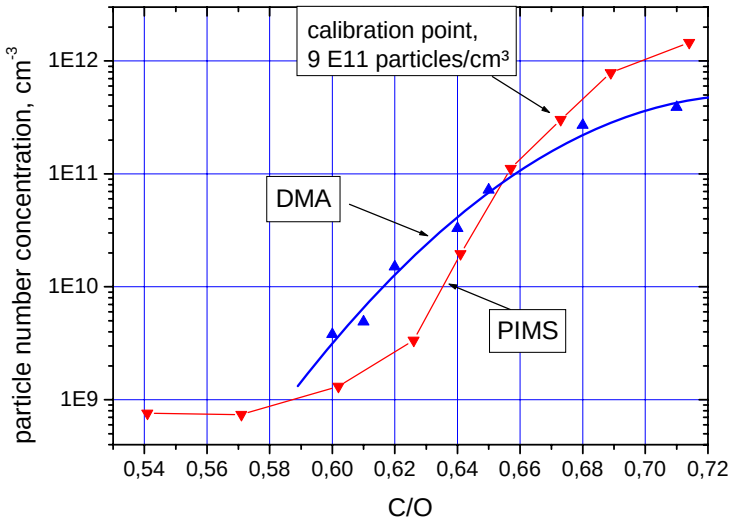
particle number concentration, cm-3
1E12
1E11
1E10
1E9
calibration point,
9 E11 particles/cm3
DMA
PIMS
0,54 0,56 0,58 0,60 0,62 0,64 0,66 0,68 0,70 0,72
C/O

Fig. 10

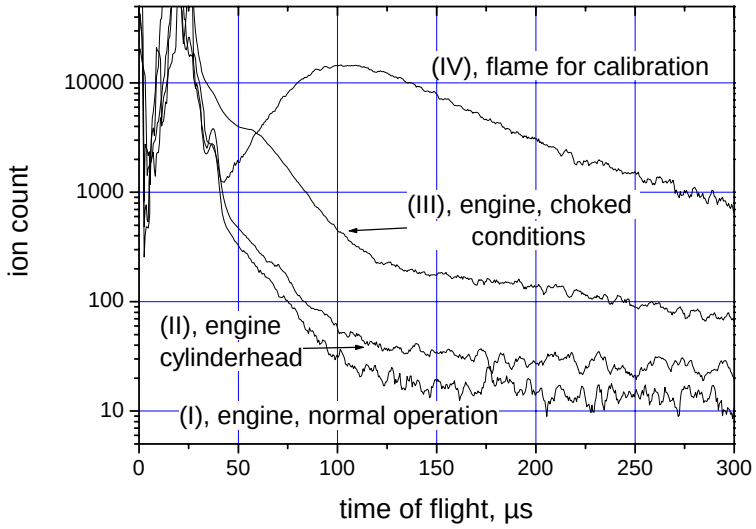
ion count
10000
1000
100
10
0
50
100
150
200
250
300
time of flight, µs
(IV), flame for calibration
(III), engine, choked conditions
(II), engine cylinderhead
(I), engine, normal operation

Fig.11

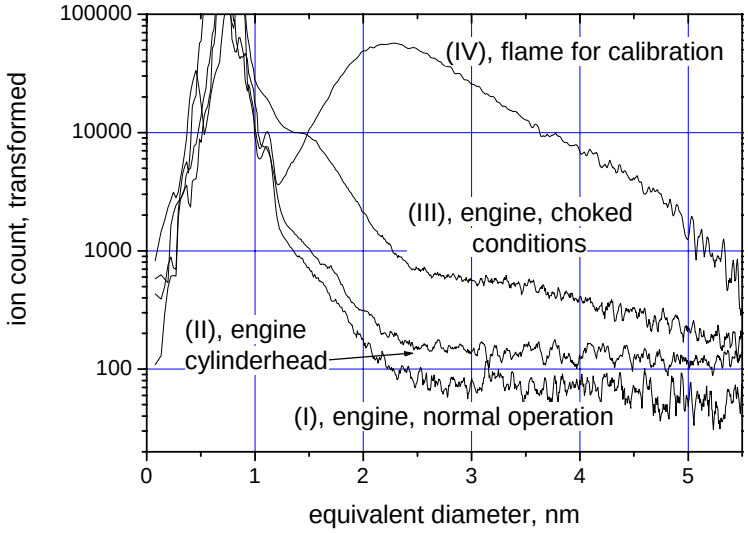
ion count, transformed
100000
10000
1000
100
0
1
2
3
4
5
equivalent diameter, nm
(IV), flame for calibration
(III), engine, choked conditions
(II), engine cylinderhead
(I), engine, normal operation

Fig. 12

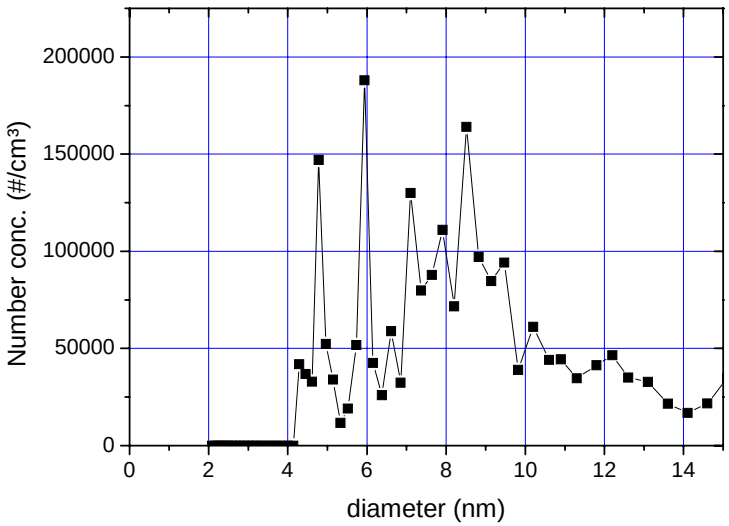

Fig. 13

C/O	**av. diameter**	**number conc.**	**number conc. corr.**
0,6	2,42	7,8 E8	3,8 E9
0,61	2,75	1,10 E9	4,9 E9
0,62	2,87	3,4 E9	1,51 E10
0,64	3,05	8,2 E9	3,3 E10
0,65	3,65	1,62 E10	7,2 E10
0,68	4,79	6,1 E10	2,7 E11
0,71	5,32	9,0 E10	3,9 E11

Table 1: Results of the DMA flame measurements